Dalton Transactions

An international journal of inorganic chemistry

Accepted Manuscript

This article can be cited before page numbers have been issued, to do this please use: R. Vilar, A. Torres Huerta, T. G. Chan and A. J. P. White, *Dalton Trans.*, 2020, DOI: 10.1039/D0DT00930J.




ROYAL SOCIETY OF CHEMISTRY

rsc.li/dalton

View Article Online
DOI: 10.1039/D0DT00930J

# Molecular recognition of bisphosphonate-based drugs by di-zinc receptors in aqueous solution and on gold nanoparticles

Aaron Torres-Huerta,[1] Tiffany G. Chan, [1] Andrew J.P. White, Ramon Vilar*[1].

[1]*Department of Chemistry, Imperial College London, White City Campus, London W12 OBZ (UK)*

Corresponding author: r.vilar@imperial.ac.uk

**Abstract**

Metal-based anion receptors have several important applications in sensing, separation and transport of negatively charged species. Amongst these receptors, di-zinc(II) complexes are of particular interest for the recognition of oxoanions, in particular phosphate derivatives. Herein we report the synthesis of a di-zinc(II) receptor and show that it has high affinity and selectivity for bisphosphonates such as alendronate and etidronate – which are used to treat a number of skeletal disorders as well as showing interesting anticancer properties. The binding mode of the di-zinc(II) receptor with alendronate and etidronate has been unambiguously established by single crystal X-ray crystallography. In addition, by modifying the backbone of the receptor, we show that the drug-loaded receptor can be attached onto gold nanoparticles as potential drug-delivery vehicles.

View Article Online
DOI: 10.1039/D0DT00930J



## 1. Introduction

Over the past two decades, there has been great interest in the development of molecular receptors for oxoanions such as carboxylates, phosphates and nitrates, amongst several others. [1] Such receptors have been designed for a wide range of applications such as sensing,[2] removal of pollutants from solutions[3] and to transport anionic guests across biological membranes.[4] One large family of such receptors is based on metal complexes with the ability to coordinate reversibly to the target anionic guest.[5] Depending on the number and nature of the metal ion as well as its coordination environment, it is possible to tune the selectivity of metallo-receptors for a given oxoanion.[6] For example, di-zinc(II) complexes have been shown to display high affinity for phosphate derivatives and, by tuning the coordination environment, display good selectivity for a given phosphate over other anions.[7]

One class of phosphate derivatives that attracted our attention are bisphosphonates such as etidronate and alendronate (see Scheme 1). These oxoanions act as inhibitors of osteoclastic bone resorption and are therefore used in the treatment of a variety of skeletal disorders such as Paget´s disease and osteoporosis.[8] Recent studies have also revealed that this type of bisphosphonates can induce apoptosis in tumour cells,[9,10] are synergistic with antineoplastic drugs[11] and can act as anti-angiogenic agents.[12,13] However, the use of bisphosphonates in the clinic has been limited since less than 1% of an orally administered dose is taken up by the cell.[14] This has been attributed to their negative electrostatic charge, which hinders their transport through the lipophilic cell membrane. Furthermore, bisphosphonates exhibit a short plasma half-life and are rapidly eliminated in urine.[15] To address these problems, liposomes, nanopeptides, calcium phosphate-DNA nanoparticles and nanopolymers have been explored as drug carriers.[16-22]

View Article Online
DOI: 10.1039/D0DT00930J



With this in mind, the aim of the research herein presented was to study whether di-zinc(II) complexes could act as good receptors for bisphosphonates and whether it would be possible to attach such host-guest systems to gold nanoparticles (AuNP) as nanocarriers for future biological applications. Thus, we report the synthesis of the di-zinc(II) molecular receptor **2** (see Scheme 1) and its interactions with etidronate and alendronate. The binding process has been studied by spectroscopic techniques (i.e. UV-vis and $^{31}$P NMR spectroscopy) and the exact binding mode of both bisphosphonates to the receptor has been established by X-ray crystallography. Furthermore, the drug-loaded metallo-receptor was further functionalised with dithiocarbamate and successfully attached onto AuNPs (see Scheme 2).

## Results and Discussion

**Synthesis and spectroscopic characterization of di-zinc(II) complex 2.** The bis(zinc(II)-dipicolylamine) motif has been used extensively in receptors for several oxoanions such as phosphates and carboxylates.[23, 24] There is also one previous example where this type of complex has been incorporated into a receptor for bisphosphonates.[25] Therefore, we synthesised the di-zinc(II) receptor **2** (see Scheme 1) and explored its ability to selectively recognise alendronate and etidronate over several other anions. In addition to the di-zinc recognition moiety, the complex also contains a benzylamine substituent since it can be readily converted into a dithiocarbamate which in turn would render the complex suitable for attachment to gold nanoparticles (see below).

Ligand **1** was obtained following a synthetic procedure previously reported for similar bis-dipicolylamine compounds (see Scheme S1).[26] Metallo-receptor **2** was synthesized by reacting **1** with two equivalents of $Zn(OAc)_2$ and one equivalent of $NaBF_4$ (see Scheme 1).

View Article Online
DOI: 10.1039/D0DT00930J

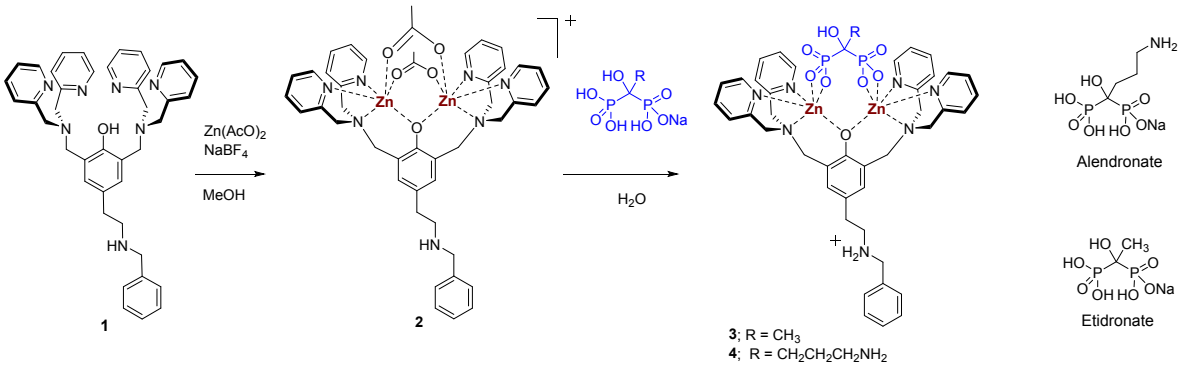


**Scheme 1**: Synthetic route for the preparation di-zinc(II) receptor **2** and its complexes with bisphosphonate-based drugs (i.e. etidronate and alendronate). Complex **3** is electrostatically neutral due to the protonation of the benzyl amine group while complex **4** is +1 due to the protonation of both the benzylamine and the amine of alendronate.

The $^{1}$H and $^{13}$C NMR spectrum of complex **2** (as compared to **1**) shows that the pyridine C/H are in two different chemical environments due to the coordination to the zinc(II) centres (see Figures S1 – S4 for $^{1}$H and $^{13}$C NMR spectra; S5 – S8 for 2D NMR spectra). In the $^{13}$C NMR spectrum, ligand **1** shows singlets at 149.0 (C1-py), 136.6 (C3-py), 123.1 (C2-py), 122.1 (C4-py) while complex **2** displays double signals for all of them, i.e. at 148.1 and 146.1 (C1-py), 139.1 and 137.7 (C3-py), 124.1 and 123.6 (C2-py), 122.7 and 121.0 (C4-py) – see ESI for numbering of atoms). The observed splitting of the $^{1}$H and $^{13}$C NMR resonances is consistent with what has been previously reported for other Zn-bis-dipicolylamine complexes.[27]

**Indicator displacement assays (IDA) and UV/vis titrations.** To study whether **2** could act as a molecular receptor for bisphosphonate-based drugs, its interaction to etidronate and alendronate was investigated via IDA. The interaction of **2** with several other anions which are physiologically relevant (i.e. $HP_2O_7^{3-}$, $HPO_4^{2-}$, $SO_4^{2-}$, $SO_3^{2-}$, $CO_3^{2-}$, $NO_3^{-}$, $OH^{-}$ and $Cl^{-}$) was also studied to establish its selectivity profile. This was performed using pyrocatechol violet (PV) as an indicator, which is yellow when free in solution but blue when coordinated

View Article Online
DOI: 10.1039/D0DT00930J



to zinc(II). Compound **2** (50 μM) was mixed with one molar equivalent of PV and the resulting **2·PV** complex was individually incubated with one molar equivalent of each anion. Upon mixing with etidronate and alendronate, an instantaneous colour change was observed, indicating the displacement of the dye by the bisphosphonate drugs (Figure 1a). In contrast, mixing **2·PV** with the other anions under study did not generate a significant change in the colour of the original solution (Figure 1a). The same experiment was repeated using 10 equivalents of each anion; in this case, besides etidronate and alendronate, pyrophosphate also induced a colour change (consistent with previous reports showing that at high concentrations pyrophosphate binds to this type of di-zinc(II) receptors – see Figure S30).

Following this initial screening, the interaction between **2·PV** and the anions was further analysed by UV-Vis spectroscopy, which confirmed the ability of receptor **2** to bind etidronate and alendronate with high selectivity over all other anions investigated – except pyrophosphate which also shows some binding at high concentrations (Figure 1b).

View Article Online
DOI: 10.1039/D0DT00930J



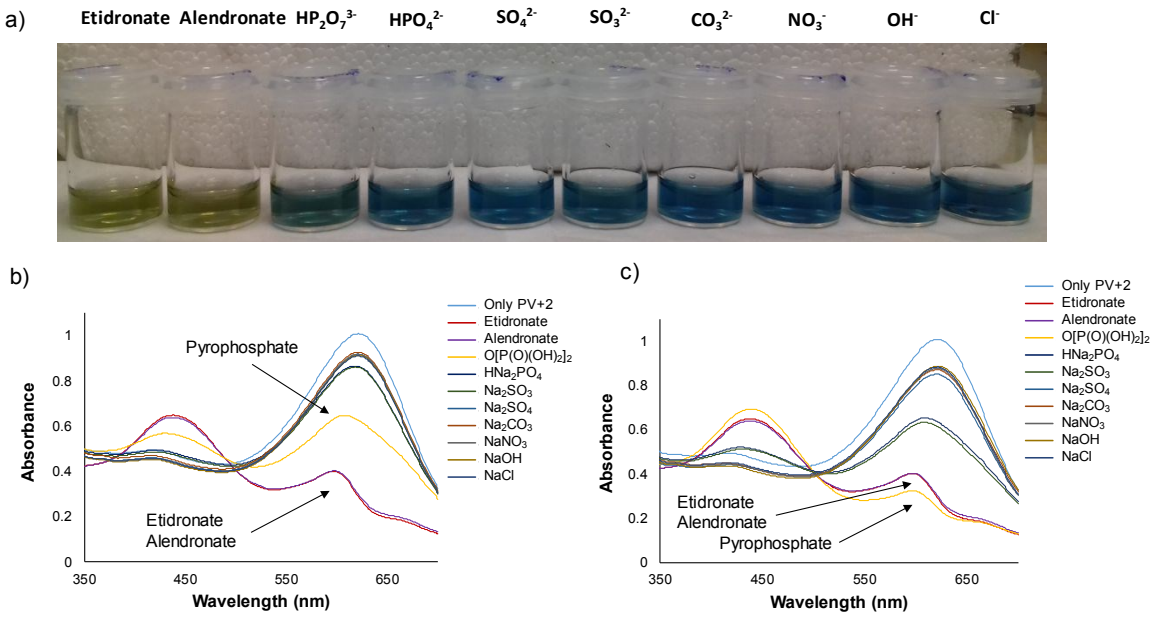


**Figure 1**: Colorimetric response of **2·PV** to different anions in 10 mM HEPES solution at pH 7.4 at room temperature. (a) With 1 eq of anions. (b) UV-Vis spectra of 50 µM **2·PV** in 10 mM HEPES solution at pH = 7.4 and 1 eq of anions (c) UV-Vis spectra of 50 µM **2·PV** in 10 mM HEPES solution at pH = 7.4 and 1 eq. of etidronate, alendronate and 10 equivalents of common inorganic anions.

Quantitative determination of the binding affinity between receptor **2** and the bisphosphonate drugs was assessed by UV-Vis and $^{31}$P NMR titrations (Figure 2). The UV-Vis titration was performed by adding increasing amounts of either etidronate or alendronate to a solution of **2·PV** (50 µM). The intensity of the UV-Vis bands centred at 455 nm increases while the band centred around 650 nm decreases upon addition of the bisphosphonate anion (Figure 2b). From this data, the association constants for **2** with etidronate ($K_a$ = 2.42±0.15 x $10^5$ $M^{-1}$) and alendronate (2.25±0.16 x $10^5$ $M^{-1}$) were calculated.

The interaction between **2** and the two drugs was also studied by $^{31}$P NMR spectroscopy in $D_2O$ at room temperature (Figure 2d). Upon addition of alendronate to a solution of **2**, a resonance at 21.9 ppm (assigned to coordinated alendronate) appeared and increased with subsequent additions of the anion until *ca*. 1 equivalent. Subsequent additions led to the appearance of a second resonance (17.8 ppm) corresponding to free bisphosphonate (similar

View Article Online
DOI: 10.1039/D0DT00930J



results were obtained for etidronate, Figure S31). The UV-Vis and $^{31}$P NMR spectroscopic studies indicate that **2** binds to etidronate and alendronate in a 1:1 stoichiometry. To confirm this, the method of continuous variation (i.e. Job's plots) was applied; as can be seen in Figure 2c and S30c, these studies clearly show the presence of a 1:1 binding stoichiometry.

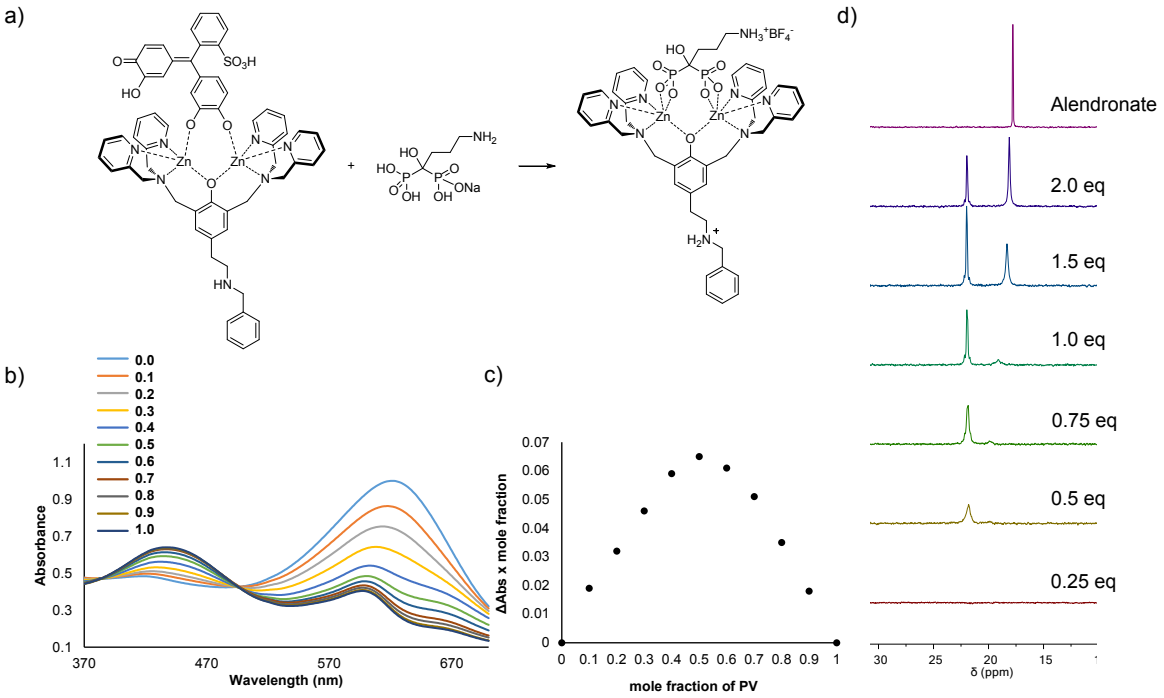


**Figure 2**: (a) Indicator displacement assay between **2·PV** and alendronate; (b) UV spectra of 50 μM **2·PV** titrated with increasing amounts of 1.25 mM alendronate in 10 mM HEPES solution, pH = 7.4. (c) Job´s plot of 50 μM **2·PV** and alendronate in 10 mM HEPES solution at pH = 7.4. (d) $^{31}$P NMR (400 MHz, $D_2O$) spectra showed the titration of **2** with alendronate.

**Synthesis of complexes 3 and 4.** Having established that receptor **2** interacts strongly with etidronate and alendronate, host-guest complexes **3** and **4** were prepared, isolated and fully characterized (including determination of their X-ray crystal structures – see below). The $^{1}$H NMR spectra of these complexes showed the disappearance of the acetate groups (i.e. the original anion in **2**) and the appearance of new resonances at 1.64 ppm and between 1.87 and 3.05 ppm associated to etidronate and alendronate, respectively. In addition, the $^{31}$P NMR

View Article Online
DOI: 10.1039/D0DT00930J



spectra of both these complexes in MeOD showed two doublets for the phosphorus of the etidronate and alendronate in the range of 23.4-24.8 and 21.9-22.9 ppm, respectively. It is interesting to note that there are differences in the $^{31}$P NMR spectra of **3** and **4** when recorded in $D_2O$ (see Figure 2d) and MeOD (see Figures S10 and S12). In the former a single resonance is observed, while in MeOD two distinct doublets are observed, which is consistent with the two different phosphorous environments (coupling to each other). The formulation and purity of these host-guest complexes were confirmed by mass spectrometry and elemental analyses (see Experimental Details).

**Single-crystal X-ray diffraction analysis.** The molecular structures of compounds **3** and **4** were determined by single-crystal X-ray crystallography (Figures 3 and 4) confirming the 1:1 association between the receptor and bisphosphonates. Suitable crystals of compounds **3** and **4** were grown from acetone and methanol/toluene solutions respectively. In both of these structures, the four negative charges of the bisphosphonate groups are delocalized between the four oxygen atoms coordinated to the zinc(II) centres and the two remaining uncoordinated oxygen atoms. This effect is evidenced in the relatively narrow distribution of the P–O distances, from 1.510(2) Å to 1.546(3) Å and 1.518(3) Å to 1.543(3) Å for **3** and **4**, respectively. These values are intermediate to the standard bond lengths reported for P–O (1.50 Å) and P=O (1.63 Å). The average values for the N–Zn, $O_{drug}$–Zn and $O_{ligand}$–Zn bond distances are 2.210 Å, 2.063 Å, 2.100 Å for **3**, and 2.212 Å, 2.059 Å, 2.096 Å for **4**. In both structures the coordination geometry around the zinc(II) centres corresponds to a distorted octahedron. In **4**, the amine group of the coordinated alendronate is protonated giving an overall positive charge to the complex.

View Article Online
DOI: 10.1039/D0DT00930J



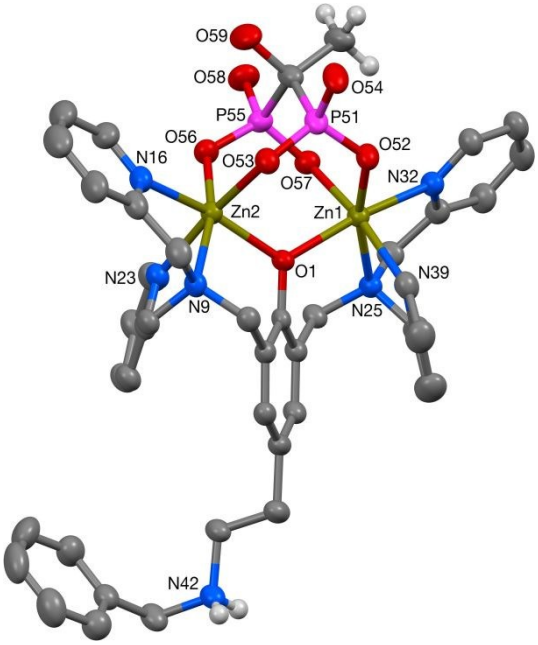


**Figure 3.** The crystal structure of **3** (50% probability ellipsoids) showing the interaction between the di-zinc(II) receptor and etidronate.

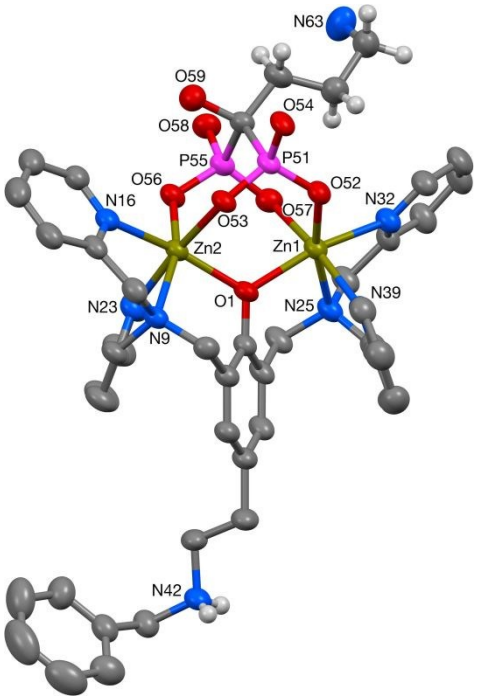


**Figure 4.** The structure of the cation in the structure of **4** (50% probability ellipsoids) showing the interaction between the di-zinc(II) receptor and alendronate.

View Article Online
DOI: 10.1039/D0DT00930J



**Functionalization of gold nanoparticles with receptors.** The next aim of this work was to explore the attachment of receptor **2** (loaded with bisphosphonates) onto gold nanoparticles (AuNP) to yield a potential drug delivery system. As has been previously reported, dithiocarbamates are efficient groups for the attachment of small molecules onto gold nanoparticles. Thus, we functionalized the backbone of receptor **2** with a dithiocarbamate to yield **5** as shown in scheme 2.

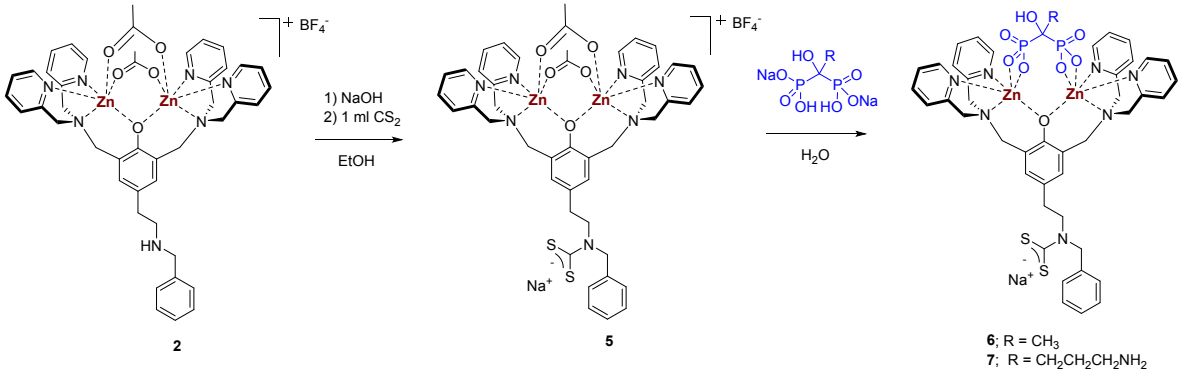


**Scheme 2**: Synthetic route for the preparation of dithiocarbamate-modified di-zinc(II) receptor and the corresponding complexes with etidronate and alendronate.

Subsequently, the modified receptor **5** was loaded with either etidronate or alendronate to yield compounds **6** and **7** respectively. Due to the limited solubility of **6** and **7**, it was not possible to obtain $^{1}H$ and $^{13}C$ NMR spectra of good enough quality to assign all the resonances. However, the $^{31}P$ NMR spectra in MeOD of these complexes showed the expected doublets for coordinated etidronate ($\delta$ = 22.1-24.9 ppm) and alendronate ($\delta$ = 22.1-22.9 ppm). In addition, ESI(+)-MS showed the molecular ion peaks for both the host-guest complexes: $[M+H]^+$ and $[M–BF_4]^+$ at 1079.70 and 1120.12 a.m.u. for **6** and **7** respectively.

View Article Online
DOI: 10.1039/D0DT00930J





These complexes were then attached to AuNPs which were also functionalised with thiolated oligonucleotides labelled with fluorescein (FAM-DNA-SH) to give the system greater biocompatibility as well as a fluorescent tag to help determining the DNA loading on the AuNP (see below). It is well established that passivation of AuNPs with a dense layer of oligonucleotides (often referred to as 'spherical nucleic acids') provides nanoconjugates with good solubility profile, low cytotoxicity and cell permeability.[28] Therefore, the following systems were prepared and studied (see Figure 5): AuNPs without receptor **2** or drug (**AuNP-DNA** – as a control), with receptor **2** but no drug (**AuNP-DNA-5**), and with drug-loaded receptor complexes **6** or **7** (**AuNP-DNA-6** and **AuNP-DNA-7**).

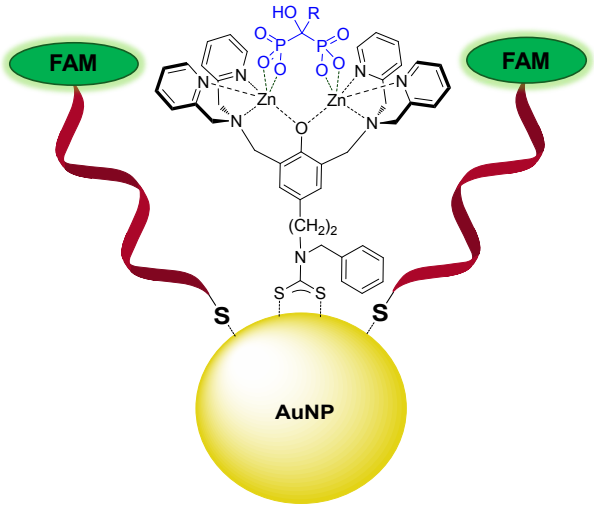


**AuNP-DNA-6**; R = $CH_3$
**AuNP-DNA-7**; R = $CH_2CH_2CH_2NH_2$

**Figure 5**: Schematic representation of nanoconjugates **AuNP-DNA-6** and **AuNP-DNA-7**.

The AuNPs were synthesized following previously reported procedures.[29] Briefly, they were grown through the reduction of $HAuCl_4$ with sodium citrate and tannic acid to yield quasi-spherical, narrowly-dispersed AuNPs with an average core diameter of 10.59 ± 1.8 nm. The characterization of the AuNPs was carried out through UV-Vis spectroscopy, dynamic light scattering (DLS), and transmission electron microscopy (TEM) (Figure S32 and Table S1).[30]

View Article Online
DOI: 10.1039/D0DT00930J



Three different methods were studied to passivate the AuNPs with thiolated fluorescein-labelled oligonucleotides and the receptor-drug **6**: (i) by first preparing **AuNP-DNA** and then adding **6** to the nanoparticles; (ii) by adding FAM-DNA-SH and **6** at the same time to the unfunctionalized AuNPs; (iii) by first adding **6** to the AuNPs and then the FAM-DNA-SH. The changes observed in the hydrodynamic diameter ($d_h$) and zeta potential ($\zeta$) of the NPs after functionalization (see Table S3) suggest that all three methods yield AuNPs passivated with both the oligonucleotides and receptor-drug conjugate **6**. However, a higher oligonucleotide loading – which, in turn, increases the stability and biocompatibility of the systems – was observed by adding the FAM-DNA-SH and receptor-drug complex together – i.e. second method described above. The oligonucleotide loading was estimated by treating the corresponding DNA-passivated AuNPs with a large excess of mercaptoethanol following reported protocols.[31] Incubation with mercaptoethanol displaces the fluorescently-labelled oligonucleotides from the AuNP surface, allowing the number of oligonucleotides attached per AuNP to be calculated.

Having established the best synthetic method, samples of **AuNP-DNA-5** and **AuNP-DNA-7** (in addition to **AuNP-DNA-6** as described above) were prepared and fully characterised by UV-Vis and fluorescence spectroscopy, DLS, TEM and inductively coupled plasma mass spectrometry (ICP-MS). The coating of AuNPs with FAM-DNA-SH to yield **AuNP-DNA** induces a change $d_h$ from 21.4 ± 0.2 nm to 45.7 ± 0.4 nm, and a change $\zeta$ from -34.8 ± 1.2 mv to -81.2 ± 0.9 mV. Addition of the complexes (**6** and **7**) makes $\zeta$ less negative which is consistent with less DNA being present on the surface of the AuNPs (see Table S3 in the ESI). The largest difference is observed for **AuNP-DNA-7** (with $\zeta$ = -25.4 ± 1.6 *cf.* -81.2 ± 0.9 for **AuNP-DNA**) which can be attributed to alendronate's positively charged alkyl

View Article Online
DOI: 10.1039/D0DT00930J



ammonium group. Additionally, there were changes in the UV-Vis absorbance of the nanoparticles before and after functionalisation, which reflects the changes of optical properties of AuNPs caused by the coating process (Figure 6a).[30] The TEM images showed that the spherical morphology of the AuNPs is preserved after the formation of the **AuNP-DNA-6** and **AuNP-DNA-7** (Figure 6c and 6d).

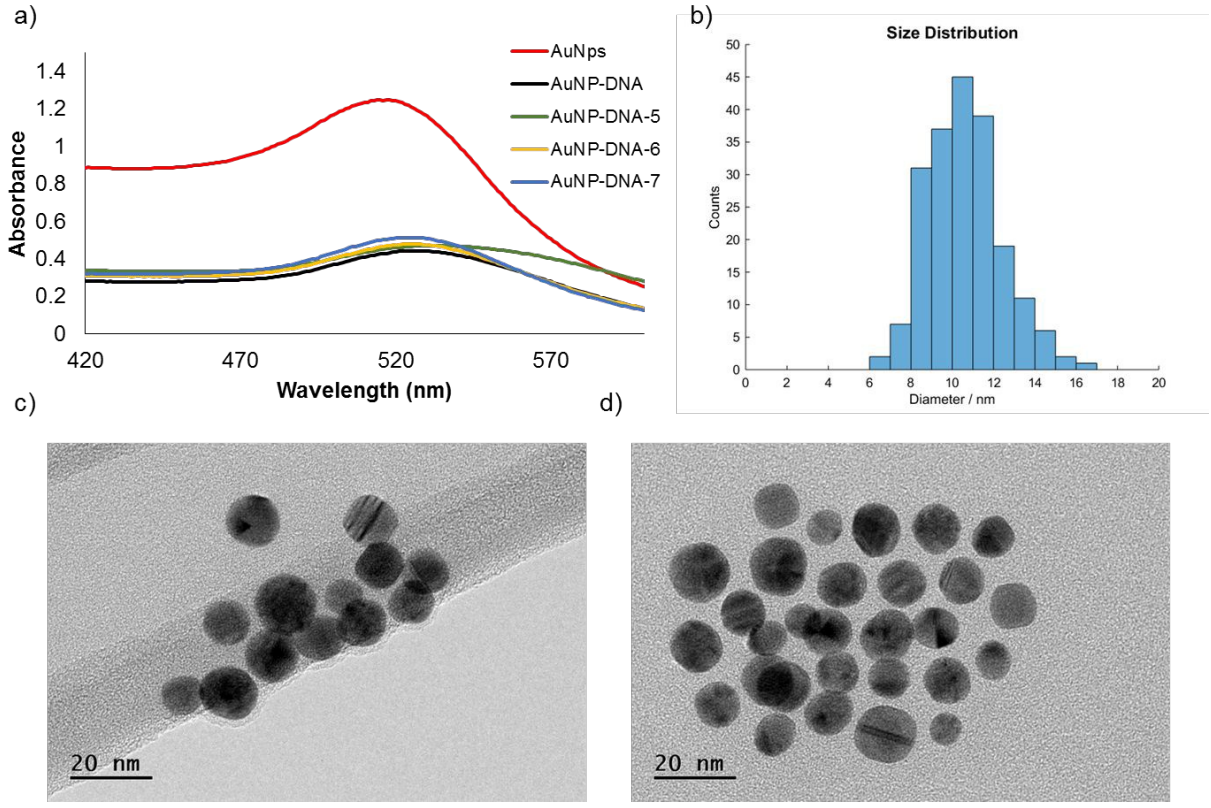


**Figure 6**: (a) UV-Vis spectra of **AuNPs**, **AuNP-DNA**, **AuNP-DNA-5**, **AuNP-DNA-6** and **AuNP-DNA-7**; (b) Size distribution of unfunctionalised **AuNPs**; and TEM of images of (c) **AuNP-DNA-6** and (d) **AuNP-DNA-7**.

Subsequently, the number of FAM-DNA molecules attached to the AuNPs was determined by fluorescence spectroscopy (as described above using mercaptoethanol) while the number of attached host-guest complexes was indirectly determined by quantifying the amount of Zn

View Article Online
DOI: 10.1039/D0DT00930J



via ICP-MS (see Table 1). These measurements indicate that there are 69 and 79 molecules of etidronate and alendronate per AuNP in **AuNP-DNA-6** and **AuNP-DNA-7** respectively. Interestingly, in the **AuNP-DNA-5**, **AuNP-DNA-6** and **AuNP-DNA-7** samples, a higher oligonucleotide loading was observed in comparison with **AuNP-DNA** sample. This effect could be attributed to the stabilization of the negative charge of oligonucleotides strands by the presence of the complexes.

**Table 1**: Samples **AuNP-DNA**, **AuNP-DNA-5**, **AuNP-DNA-6** and **AuNP-DNA-7**

| | **AuNP-DNA** | **AuNP-DNA-5** | **AuNP-DNA-6** | **AuNP-DNA-7** |
|---|---|---|---|---|
| **DNA-Concentration** | 0.42 µM | 0.61 µM | 0.64 µM | 0.7 µM |
| **DNA-molecules** | 54 | 78 | 82 | 90 |
| **Zn-Concentration** | n/a | 206.4 µg/L (3.2 µM) | 141.6 µg/L (2.2 µM) | 161.5 µg/L (2.5 µM) |
| **Zn-atoms** | n/a | 200 | 138 | 157 |
| **Drug-concentration** | n/a | n/a | 1.1 µM | 1.2 µM |
| **Drug-molecules** | n/a | n/a | 69 | 79 |

Note: The initial concentration of AuNPs was 12.1 nM. After addition of thiolated oligonucleotide and the corresponding compounds, the final concentration of AuNPs was 7.8 nM.

## Conclusions

In summary, we have shown that di-zinc(II) complex **2** binds bisphosphonates with high affinity and good selectivity over many other physiologically-relevant anions. The X-ray crystal structures of this receptor bound to alendronate and etidronate show for the first time the exact binding mode of these oxoanions to a di-metallic receptor. We also show that by

View Article Online
DOI: 10.1039/D0DT00930J



modifying the backbone of the receptor, it is possible to load the drug-loaded receptor onto AuNPs that have also been passivated with oligonucleotides to make them water-soluble and biocompatible. These new nanoconjugates are likely to be good vehicles for the delivery of these drugs across the cell membrane. Future work will explore this possibility.

## Experimental Section

### General Information.

$^{1}$H NMR, $^{13}$C NMR and $^{31}$P NMR spectra were recorded on either a Bruker Avance 400 MHz Ultrashield NMR spectrometer or a Bruker Avance 500 MHz NMR spectrometer. Electrospray ionisation mass spectra were obtained on a Bruker Daltonics Esquire 3000 spectrometer. The X-ray crystal structures where measured using an OD Xcalibur PX Ultra Diffractometer (1.54184 Å). UV-Vis spectra were collected with a Perkin Elmer UV-Vis Lambda 25 Spectrophotometer. Fluorescence measurements were made on a Cary Eclipse Fluorescence Spectrophotometer. Hydrodynamic diameters and zeta potentials were measured on a Malvern Zetasizer Nano ZS instrument. Nanoparticles images were taken using a JEOL JEM-2100 Plus transmission electron microscope. All reagents were purchased from commercial suppliers and used without further purification. Etidronate and alendronate were purchased as etidronate disodium hydrate and alendronate sodium trihydrate, respectively. The organic precursor **d** was prepared following a previously reported synthetic procedure (Scheme S1).[26] For numbering of the $^{1}$H NMR assignments shown below, please see the corresponding spectra in the ESI.

View Article Online
DOI: 10.1039/D0DT00930J



**Synthesis of Compound 1:** To a solution of **d** (0.815 g, 1.45 mmol) in methanol (20 mL) benzaldehyde (0.177 mL, 1.74 mmol) was added dropwise. The reaction mixture was stirred for 2 h at room temperature. $NaBH_4$ (110g, 2.90 mmol) was then added to the reaction mixture and after stirring it for 4 h, the solvent was removed under vacuum and the excess $NaBH_4$ neutralised with saturated $NH_4Cl$ aqueous solution (60 mL). The product was extracted with dichloromethane and dried over $Na_2SO_4$ powder. After filtration, the solvent was reduced under vacuum to yield a brown oil which was purified by silica column chromatography with $CHCl_3$/MeOH/$Et_3N$ (94:5:1) as eluent to afford ligand **1** as a yellow oil. Yield: 87 % (0.819 g, 1.26 mmol). $^1$H NMR (400 MHz, $CDCl_3$) δ 2.72 (t, *J* = 7.0 Hz, 2H, H12), 2.82 (t, *J* = 7.0 Hz, 2H, H13), 3.74 (s, 2H, H14), 3.77 (s, 4H, H7), 3.85 (s, 8H, H6), 6.97, 7.02, 7.10, 7.22, 7.48, 7.54 (m, 18H, *H* of Ph, Ar and Py groups), 8.49 (s, 4H, H1), 10.89 (s, 1H, O*H*) ppm. $^{13}$C{$^1$H} NMR (101 MHz, $CDCl_3$) δ 35.5 (C12), 51.0 (C13), 54.0 (C14), 55.0 (C7), 60.0 (C6), 122.1, 123.1, 123.3, 124.2, 127.0, 128.2, 128.5, 129.5, 136.6, 140.2, 149.0, 154.4, 159.4 (*C* of ph, Ar and Py groups) ppm. High-resolution ES-MS for $C_{41}H_{44}N_7O$ (calcd 650.3607): m/z (%) = 650.3625 (100) (M+H, 100; error 2.8 ppm).

**Synthesis of Compound 2**: To a mixture of **1** (0.465 g, 0.71 mmol) and zinc(II) acetate dihydrate (0.313 mg, 1.43 mmol) methanol (30 mL) was added and left stirring for 2 h at room temperature. $NaBF_4$ (0.078g, 0.71 mmol) was subsequently added and the resulting reaction mixture was stirred overnight. After this time, all the volatiles was removed under reduce pressure. The remaining solid was washed three times with ethyl acetate (60 ml) and the product was extracted with dichloromethane to afford compound **2** as a slightly yellow solid. Yield: 90 % (0.630 g, 0.64 mmol). Elemental analysis (%) Calcd for

View Article Online
DOI: 10.1039/D0DT00930J



$C_{45}H_{48}BF_4N_7O_5Zn_2 \cdot CH_2Cl_2$ (1069.40 g·mol$^{-1}$): C 51.66, H 4.71, N 9.17; Found: C 51.16, H 4.68, N 8.97. FT-IR (ATR) $\tilde{\nu}$ (cm$^{-1}$)1604 (s), 1481 (m), 1414 (s), 1325 (w), 1295 (w), 1098 (m), 1053 (s), 1020 (s), 964 (w), 767 (m). $^1$H NMR (400 MHz, $CDCl_3$) δ 2.02 (s, 6H, H20), 2.54 (m, 2H, H12), 2.81 (m, 2H, H13), 3.20 (d, *J* = 11.1 Hz, 2H, H6d), 3.32 (m, 4H, H7b, NH), 3.50 (d, *J* = 16.1 Hz, 2H, H7a), 3.81 (d, *J* = 11.0 Hz, 2H, H6c), 3.95 (s, 2H, H14), 3.98 (d, *J* = 14.4 Hz, 2H, H6b), 4.51 (d, *J* = 14.4 Hz, 2H, H6a) 6.31 (d, *J* = 7.7 Hz, 2H, H4b), 6.49 (s, 2H, H10), 6.90 – 7.45 (m, 13H, H2b, H3b, H2a, H17, H18, H16, H4a), 7.83 (t, *J* = 8.5 Hz, 2H, H3a), 8,18 (d, *J* = 4.5 Hz, 2H, H1b), 8.83 (d, *J* = 4.5 Hz, 2H, H1a) ppm. $^{13}$C{$^1$H} NMR (101 MHz, $CDCl_3$) δ 24.6 (C20), 33.4 (C12), 50.3 (C13), 52.7 (C14), 57.8 (C7), 60.1 (C6), 121.0, 122.7, 123.6, 123.9, 124.1, 125.8, 127.9, 128.8, 129.1, 131.2 (C4b, C4a, C2a, C2b, C9, C15, C11, C16, C17, C18, C10), 137.7, 139.1 (C3a, C3b), 146.1, 148.1 (C1a, C1b), 154.6, 155.1 (C5a, C5b), 160.1 (C8), 178.8 (C19) ppm. ES-MS: m/z (%) = 872.2 (60) [M – $BF_4$ – $CCH_3$]$^+$.

**Synthesis of Compound 3**: To a solution of **2** (0.200 g, 0.20 mmol) in water (30 ml), a solution of etidronate disodium hydrate (0.054 g, 0.20 mmol) in water (2 ml) was added dropwise. The resulting reaction mixture was stirred overnight. After this time, the solvent was reduced under vacuum to *ca*. 5 ml. At this point, a white precipitate formed which was filtered and then washed with chloroform and acetone. Crystals of compound **3** were grown from acetone at room temperature. Yield: 88 % (0.176 g, 0.20 mmol). Elemental analysis (%) Calcd for $C_{43}H_{47}N_7O_8P_2Zn_2 \cdot 2H_2O$ (1018.61 g·mol$^{-1}$): C 50.70, H 5.05, N 9.63; Found: C 50.40, H 5.01, N 9.34. FT-IR (ATR) $\tilde{\nu}$ (cm$^{-1}$)1608 (w), 1481 (w), 1442 (w), 1154 (m), 1053 (s), 1020 (s), 927 (w), 767 (w). $^1$H NMR (400 MHz, MeOD) δ 1.64 (t, *J* = 14.8 Hz, 3H),

View Article Online
DOI: 10.1039/D0DT00930J



2.95–2.57 (m, 6H), 3.12 (m, 2H), 3.45 (m, 2H), 4.17–3.98 (m, 6H), 4.65 (m, 2H), 6.44–6.35 (m, 4H,), 7.41 (m, 13H), 7.88 (t, $J$ = 7.6 Hz, 2H), 8.81 (m, 4H) ppm. $^{31}$P NMR (400 MHz, MeOD) δ 23.4 (d, $J$ = 36.5 Hz, 1P), 24.8 (d, $J$ = 36.5 Hz, 1P) ppm. ES-MS: m/z (%) = 989.1 (20) $[M–CH_3+Na]^+$.

**Synthesis of Compound 4**: Compound **4** was synthesized using the same methodology described for **3**. Crystals of compound **4** were grown from methanol/toluene solution at room temperature. Yield: 64 % (0.290 g, 0.26 mmol). Elemental analysis (%) Calcd for $C_{45}H_{53}BF_4N_8O_8P_2Zn_2·4H_2O$ (1185.52 g·mol$^{-1}$): C 45.59, H 5.19, N 9.45; Found: C 45.20, H 4.95, N 9.05. FT-IR (ATR) $\tilde{\nu}$ (cm$^{-1}$)1608 (w), 1477 (w), 1442 (w), 1319(w), 1290 (w), 1078 (s), 1050 (s), 1020 (s), 933 (m), 763 (m). $^1$H NMR (400 MHz, MeOD) δ 1.87 (m, 3H), 2.30–3.05 (m, 14H), 3.73–4.21 (m, 8H), 4.73 (m, 3H), 6.25–6.38 (m, 4H), 6.96–7.35 (m, 13H), 7.85 (m, 2H), 8.82–8.89 (m, 4H) ppm. $^{31}$P NMR (400 MHz, MeOD) δ 21.9 (d, $J$ = 30.7 Hz, 1P), 22.9 (d, $J$ = 31.1 Hz, 1P). ES-MS: m/z (%) = 1025.2 (15) $[M–BF_4]^+$.

**Synthesis of Compound 5**: To a solution of **2** (1.00 g, 1.01 mmol) in ethanol (10 ml) NaOH (0.04 g, 4.04 mmol) was added and left stirring for one hour at room temperature. Subsequently, an excess of $CS_2$ (1 ml) was added to the mixture and a white precipitate formed immediately. The reaction was left stirring for two more hours. After this time, the solvent was removed under reduce pressure and the resulting crude solid dissolved in acetone. The solution was then filtered and hexane added to the filtrate to yield a white precipitated which was filtered and dried under vacuum. Yield: 71 % (0.777 g, 0.72 mmol).

View Article Online
DOI: 10.1039/D0DT00930J



Elemental analysis (%) Calcd for $C_{46}H_{49}BF_4N_7NaO_5S_2Zn_2$ (1084.61 g·mol$^{-1}$): C 50.94, H 4.55, N 9.04; Found: C 50.41, H 4.54, N 8.80. FT-IR (ATR) $\tilde{\nu}$ (cm$^{-1}$)1604 (s), 1578 (m), 1481 (m), 1418 (m), 1323, (w), 1295 (w), 1098 (m), 1057 (s), 1024 (s), 964 (w), 771 (m). ES-MS: m/z (%) = 957.1 (25) $[M–CH_3–Na–BF_4]^+$.

**Synthesis of Compound 6**: A solution of **5** in water (10 ml) was stirred for 30 minutes. Subsequently, etidronate dissolved in 3 ml of water was added dropwise and the resulting reaction mixture was left sitting for 4 hours. After this time, the solvent was reduced to 3 ml and a white precipitate formed which was filtered and washed with acetone, diethyl ether and hexane. Yield: 90 % (0.359 g, 0.33 mmol). Elemental analysis (%) Calcd for $C_{44}H_{45}N_7NaO_8P_2S_2Zn_2·2H_2O$ (1115.73 g·mol$^{-1}$): C 47.37, H 4.43, N 8.79; Found: C 47.20, H 4.15, N 8.55. FT-IR (ATR) $\tilde{\nu}$ (cm$^{-1}$) 1608 (w), 1477 (w), 1444 (w), 1318 (w), 1297 (w), 1102 (s), 1053 (s), 1024 (s), 983 (m), 919 (w), 767 (w). $^{31}$P NMR (400 MHz, MeOD) δ 22.1 (br s, 1P), 24.9 (br s, 1P) ppm. ES-MS: m/z (%) = 1078.1 (80) $[M+H]^+$.

**Synthesis of Compound 7**: Compound **7** was synthesized using the same methodology described for **6**. Yield: 87 % (0.777 g, 0.72 mmol). Elemental analysis (%) Calcd for $C_{46}H_{51}BF_4N_8NaO_8P_2S_2Zn_2·5H_2O$ (1300.65 g·mol$^{-1}$): C 42.48, H 4.73, N 8.62; Found: C 42.18, H 4.60, N 8.33. FT-IR (ATR) $\tilde{\nu}$ (cm$^{-1}$) 1604 (w), 1477 (w), 1436 (w), 1319 (w), 1294 (w), 1154 (m), 1098 (s), 1072 (s), 1053 (s), 1020 (s), 957 (s), 919 (m), 886 (w), 767 (w). $^{31}$P NMR (400 MHz, MeOD) δ 22.9 (d, $J$ = 31.8 Hz, 1P), 22.1 (d, $J$ = 30.0 Hz, 1P) ppm. ES-MS: m/z (%) = 1122.1 (5) $[M–BF_4]^+$.

View Article Online
DOI: 10.1039/D0DT00930J



**Indicator displacement assays (IDAs).** All samples were freshly prepared in 10 mM HEPES buffer (pH 7.1) prior to measurements. All measurements were repeated 3 times. For optical tests, 1 ml of **2·PV** (50 μM) was mixed with 5 μL (1 eq.) or 50 μL (10 eq.) of the corresponding anion (10 mM) in 10 mM HEPES solution at pH 7.4 at room temperature. The mixture was stirred gently and then left to stand for 10 min. To obtain the UV-Vis spectra, 700 μL **2·PV** were added to a UV-Vis cuvette and mixed with one or ten molar equivalent of each anion under study in a buffer solution (10 mM HEPES at pH = 7.4) at room temperature. To obtain $K_a$ between pyrocatechol violet (PV) and compound **2**, a solution of 50 μM PV and 1.25 mM **2** were prepared. A series of solutions were prepared with increasing concentrations of **2**, keeping the indicator concentration constant. The solutions were equilibrate for 10 min before measuring the absorbance at 445 nm. The obtained data was fitted by a Benesi-Hildebrand plot. To obtain $K_a$ between **2** with the etidronate and alendronate, a fresh solution of 50 μM **2·PV** and 1 mM etidronate and 1 mM alendronate were prepared. A series of solutions were prepared with increasing concentrations of etidronate or alendronate, keeping the **2·PV** concentration constant. The association constant were obtained based on the previously described equilibrium for competition assays.[32]

**Synthesis of Gold Nanoparticles via a Seeded Growth Method.** AuNPs of different sizes were synthesized following protocols reported from Puntes *et al*.[33] Sodium citrate (25 ml, 2.2 mM), tannic acid (17 μL, 2.5 mM) and potassium carbonate (170 μL, 150 mM) was heated in a 50 mL three-necked round-bottom flask under vigorous stirring. When the temperature reached 70 °C, $HAuCl_4$ (0.41 mL, 10 mM) was injected, resulting in a color change from colorless to pink. Stirring at 70 °C for a further 10 minutes generated a solution of seed

View Article Online
DOI: 10.1039/D0DT00930J



AuNPs. To grow larger NPs, the seed solution was immediately diluted by removing 9.1 mL of the solution and replacing with sodium citrate (9.1 mL, 2.2 mM). When the temperature reached 70 °C again, two injections of $HAuCl_4$ (0.2 mL, 10 mM) on a time interval of 10 minutes were done. This growing process (sample dilution followed by the injection of $HAuCl_4$) was followed by UV-Vis spectroscopy and was repeated until the nanoparticles reached the desired size.

**Functionalization of Gold Nanoparticles.** Au NPs were functionalized with FAM-DNA-SH and the corresponding complexes (i.e. **5**, **6** or **7**) based on general methodologies previously described in the literature.[34,35] FAM-TT-GGG-TTA-GGG-TTA-GGG-TTA-GGG-TT-$(CH_2)_6$-SH (FAM-DNA-SH) oligonucleotide was selected with a thiol modifier on the 3' end and a fluorescein (as an optical label) amidite group on the 5' end. Before use, tris(2-carboxyethyl)phosphine) (TCEP) was added to FAM-DNA-SH in a 100x excess and the mixture was shaken for 1 hr at room temperature. Final concentrations of TCEP and FAM-DNA-SH were 5 mM and 50 μM respectively. 1 wt% Tween 20 (68.7 μL) was added to the AuNPs (12.1 nM, 6.87 mL) and the mixture was stirred for 1 min. FAM-DNA-SH (50 μM) and the corresponding bimetallic zinc complex (500 μM) was added at a volume that allowed for 90 and 350 oligonucleotide strands and complex per AuNP. NaCl (5 M) was then added until its final concentration in the mixture reached 800 mM. The solution was incubated for 1 h at 25 °C with gentle agitation and then centrifuged at 30,000 rpm for 15 min at 15 °C. The supernatant was removed and the NPs were redispersed in Milli-Q water. This centrifugation process was repeated at least 3 times to ensure thorough washing of the AuNPs.

View Article Online
DOI: 10.1039/D0DT00930J



**Determination of oligonucleotide loading.** 200 μL of the corresponding AuNP sample (i.e. **AuNP-DNA**, **AuNP-DNA-5**, **AuNP-DNA-6** and **AuNP-DNA-7**) were dispersed in PBS (66.6 μL) and mercaptoethanol (533.3 μL). The final concentration of mercaptoethanol was 30 mM. After stirring the reaction mixture at 25 °C for 48 h, it was centrifuged at 15,000 rpm for 15 min and the supernatant (containing the displaced oligonucleotides) was separated. The fluorescence of the FAM-DNA-SH was measured and compared to a standard curve; samples were excited at 495 nm and were scanned in the range of 500 to 650 nm. The concentration of fluorescent oligonucleotides was divided by the initial concentration of NPs to give the number of oligonucleotides attached per nanoparticle.

**Crystal data for 3**: $C_{43}H_{47}N_7O_8P_2Zn_2 \cdot 12.5(H_2O)$, $M$ = 1207.75, triclinic, $P$-1 (no. 2), $a$ = 13.6466(11), $b$ = 14.0282(7), $c$ = 16.2009(9) Å, α = 91.859(4), β = 96.471(5), γ = 117.397(7)°, $V$ = 2723.5(3) Å$^3$, $Z$ = 2, $D_c$ = 1.473 g cm$^{-3}$, μ(Cu-Kα) = 2.328 mm$^{-1}$, $T$ = 173 K, colourless blocks, Agilent Xcalibur PX Ultra A diffractometer; 10425 independent measured reflections ($R_{int}$ = 0.0459), $F^2$ refinement,[36,37] $R_1$(obs) = 0.0465, $wR_2$(all) = 0.1214, 7550 independent observed absorption-corrected reflections [$|F_o| > 4\sigma(|F_o|)$, completeness to $\theta_{full}$(67.7°) = 98.3%], 568 parameters. CCDC 1984670. See ESI for further discussion about this X-ray crystal structure.

**Crystal data for 4**: $[C_{45}H_{53}N_8O_8P_2Zn_2](BF_4) \cdot 0.5(C_7H_8) \cdot 8(H_2O) \cdot 1.5(CH_4O)$, $M$ = 1351.70, triclinic, $P$-1 (no. 2), $a$ = 12.3489(3), $b$ = 13.7028(5), $c$ = 18.1556(8) Å, α = 90.414(3), β = 93.300(3), γ = 100.305(3)°, $V$ = 3017.13(18) Å$^3$, $Z$ = 2, $D_c$ = 1.488 g cm$^{-3}$, μ(Cu-Kα) = 2.229 mm$^{-1}$, $T$ = 173 K, colourless tabular needles, Agilent Xcalibur PX Ultra A diffractometer; 11520 independent measured reflections ($R_{int}$ = 0.0349), $F^2$ refinement,[36,37] $R_1$(obs) = 0.0567,

View Article Online
DOI: 10.1039/D0DT00930J

$wR_2$(all) = 0.1796, 8585 independent observed absorption-corrected reflections [$|F_o| > 4\sigma(|F_o|)$, completeness to $\theta_{full}(67.7°) = 98.4\%$], 757 parameters. CCDC 1984671. See ESI for further discussion about this X-ray crystal structure.





**Acknowledgements**

A.T.-H. acknowledges Mexico's Consejo Nacional de Ciencia y Tecnología (CONACyT) for his postdoctoral fellowship (grant number 298826). T.G.C. acknowledges UK's Engineering and Physical Sciences Research Council (EPSRC) for her PhD Studentship (grant number EP/L016737/1).

**References**

1) a) Amendola, V.; Fabbrizzi, L.; Mosca, L. *Chem. Soc. Rev.* **2010**, *39*, 3889–3915. b) Busschaert, N.; Caltagirone, C.; Van Rossom, W.; Gale, P. A. *Chem. Rev.* **2015**, *115*, 8038–8155.

2) a) Gale, P. A.; Caltagirone, C. *Chem. Soc. Rev.* **2015**, *44*, 4212–4227. b) Pal. S.; Ghosh, T. K.; Ghosh, R.; Mondal, S.; Ghosh, P. *Coord. Chem. Rev.* **2020**, *405*, 213128–213185.

3) a) Danil de Namor, A. F.; Aparicio-Aragon, W.; Nwogu, N.; El Gamouz, A.; Piro, O. E.; Castellano, E. E. *J. Phys. Chem. B* **2011**, *115*, 6922–934. b) Albelda, M. T.; Frías, J. C.; García-España, E.; Schneider, H.-J. *Chem. Soc. Rev.* **2012**, *41*, 3859–3877.

4) Gale, P. A.; Davis, J. T.; Quesada, R. *Chem. Soc. Rev.* **2017**, *46*, 2497–2519.

5) Ngo, H. T.; Liu, X.; Jolliffe, K. A. *Chem. Soc. Rev.* **2012**, *41*, 4928–4965.

View Article Online
DOI: 10.1039/D0DT00930J



6) Tobey, S. L.; Jones, B. D.; Anslyn, E. V. *J. Am. Chem. Soc.* **2003**, *125*, 4026–4017

7) Sakamoto, T.; Ojida, A.; Hamachi, I. *Chem. Commun.* **2009**, 141–152.

8) Lewiecki E. M. *Ther. Adv. Chronic. Dis.* **2010**, *3*, 115–128.

9) Moreau, M. F.; Guillet, C.; Massin, P.; Chevalier, S.; Gascan, H.; Baslé, M. F.; Chappard, D. *Biochem. Pharmacol.* **2007**, *73*, 718–723.

10) Mitrofan, L. M.; Pelkonen, J.; Mönkkönen, J. *Bone* **2009**, *45*, 1153–1160.

11) Santini, D.; Caraglia, M.; Vincenzi, B.; Holen, I.; Scarpa, S.; Budillon, A.; Tonini, G. *Nat. Clin. Pract. Oncol.* **2006**, *3*, 325–338.

12) Hodgins, N. O.; Wang, J. T.–W.; Al–jamal, K. T. *Adv. Drug Deliver Rev.* **2017**, *114*, 143–160.

13) Green, J.; Lipton, A. *Cancer Invest.* **2010**, *28*, 944–957.

14) Watts, N. B.; Diab, D. L. *J. Clin. Endocrinol. Metab.* **2010**, *95*, 1555–1565.

15) Kimmel D. B. *J. Dent. Res.* **2017**, *86*, 1022–1033.

16) Sun, W.; Han, Y.; Li, Z.; Ge, K.; Zhang, J. *Langmuir* **2016**, *32*, 9237–9244.

17) Li, W.; Xin, X.; Jing, S.; Zhang, X.; Chen, K.; Chen, D.; Hu, H. *J. Mater. Chem. B* **2017**, *5*, 1601–1610.

18) Shmeeda, H.; Amitay, Y.; Gorin, J.; Tzemach, D.; Mak, L.; Ogorka, J.; Kumar, S.; Zhang, A.; Gabizon, A. *J. Control Release* **2010**, *146*, 76–83.

19) Li, X.; Naguib, Y. W.; Cui, Z. *Int. J. Pharm*. **2017**, *526*, 69–76.

20) Marra, M.; Salzano, G.; Leonetti, C.; Porru, M.; Franco, R.; Zappavigna, S.; Luguori, G.; Botti, G.; Chieffi, P.; Lamberti, M.; Vitale, G.; Abbruzzese, A.; La Rotonda, M. I.; De Rosa, G.; Caraglia, M. *Biotechno. Adv.* **2012**, 30, 302–309.

View Article Online
DOI: 10.1039/D0DT00930J



21) Massey, A. S.; Pentlavalli, S.; Cunningham, R.; McCrudden, C. M.; McErlean, E. M.; Redpath, P.; Ali, A. A.; Annett, S.; McBride, J. W.; McCaffrey, J.; Robson, T.; Migaud, M. E.; McCarthy, H. O. *Mol. Pharmaceutics* **2016**, *13*, 1217–1228.

22) Salzano, G.; Marra, M.; Porru, M.; Zappavigna, S.; Abbruzzese, A.; La Rotonda, M. I.; Leonettic, C.; Caraglia, M.; De Rosa, G. *Int. J. Pharm*. **2011**, *403*, 292–297.

23) Kim, S. Y.; Lee, H. D.; Hong, J.–I.; Yoon, J.; *Acc. Chem. Res.* **2009**, *42*, 23–31.

24) Liu, G.; Choi, K. Y.; Bhirde, A.; Swierczewska, M.; Yin, J.; Lee, S. W.; Park, J. H.; Hong, J. I.; Xie, J.; Niu, G.; Kiesewetter, D. O.; Lee, S.; Chen, X. *Angew. Chem. Int. Ed.* **2012**, *51*, 445–449.

25) a) Jeong, Y.; Kim, S. Y.; Jin, G.-W.; An, S.; Lee, J. H.; Jeong, A.; Chio, Y.; Hong, J.-I.; Park, J.-S. *Bull. Korean Chem. Soc.* **2010**, *31*, 2561–2564. b) Jeong, Y.; Jin, G.; Kim, S. K.; Yoon, J.; Park, J.-S. *Bull. Korean Chem. Soc.* **2011**, *33*, 37–38.

26) Moffat, C. D.; Weiss, D. J.; Shivalingam, A.; White, A. J. P.; Salaün, P.; Vilar, R. *Chem. Eur. J.* **2014**, *20*, 17168–17177.

27) Svane, S.; Kjeldsen, F.; McKee, V.; Mckenzie, C.; *Dalton Trans.* **2015**, *44*, 11877–11886.

28) a) Cutler, J. I.; Auyeung, E.; Mirkin, C. A. *J. Am. Chem. Soc.* **2012**, *134*, 1376–1391. b) Giljohann, D. A.; Seferos, D. S.; Prigodich, A. E.; Patel, P. C.; Mirkin, C. A. *J. Am. Chem. Soc.* **2009**, *131*, 2072–2073.

29) Chan, T. G.; Morse, S. V. Copping, M. J.; Choi, J. J.; Vilar, R. *ChemMedChem* **2018**, 13, 1311–1314.

30) Haiss, W.; Thanh, N. T. K.; Aveyard, J.; Fernig, D. G. *Anal. Chem.* **2007**, *79*, 4215–4221.

View Article Online
DOI: 10.1039/D0DT00930J

31) Demers, L. M.; Mirkin, C. A.; Mucic, R. C.; Reynolds, R. A.; Letsinger, R. L.; Elghanian, R.; Viswanadham, G. *Anal. Chem.* **2000**, *72*, 5535–5541.

32) Conners, K. A.; John Wiley and Sons: New York, **1987**, 175–183.

33) Piella, J.; Bastús, N. G.; Puntes, V. *Chem. Mater.* **2016**, *28*, 1066–1075.

34) Li, L.; Zhu, B.; Yao, X. Zhang, Y.; Zhu, Z.; Tu, S.; Jia, S.; Liu, R.; Kang, H.; Yang, C. J. *ACS Appl. Mater. Interfaces* **2014**, *6*, 16800–16807.

35) Chan, T. G.; Morse, S. V. Copping, M. J.; Choi, J. J.; Vilar, R. *ChemMedChem* **2018**, 13, 1311–1314.

36) SHELXTL v5.1, Bruker AXS, Madison, WI, 1998.

37) SHELX-2013, G.M. Sheldrick, *Acta Cryst.*, 2015, **C71**, 3-8.

View Article Online
DOI: 10.1039/D0DT00930J

## Graphical Abstract

Molecular recognition of bisphosphonate drugs by a di-zinc(II) receptor in solution and on gold nanoparticles is reported.